Title: **Fatigue resonant tests on drill collar rotary shouldered connections and critical thread root identification**

Authors: **C. Santus, L. Bertini, A. Burchianti, T. Inoue, N. Sakurai**

DOI Link: https://doi.org/10.1016/j.engfailanal.2018.02.027

Fatigue resonant tests on drill collar rotary shouldered connections and critical thread root identification

C. Santus[a,*], L. Bertini[a], A. Burchianti[b], T. Inoue[c], N. Sakurai[c]

[a] *DICI, Department of Civil and Industrial Engineering, University of Pisa, Italy.*
[b] *ACTA Srl, Rosignano (LI), Italy.*
[c] *JAMSTEC - CDEX, Japan Agency for Marine-Earth Science and Technology, Japan.*

Abstract

A fatigue test series on a drill collar rotary shouldered connection, thread type 5-1/2 FH MOD, was performed with a dedicated alternating bending resonant test rig. Compared to a quasi-static testing approach, the dynamic loading allowed high testing frequency and a relatively light supporting structure. Crack initiation was identified as the onset of a discrepancy between two strain gauge signals which were monitored throughout the test. A through-wall crack condition was assumed as the effective fatigue failure. The stress distribution in the connection was then analysed with a finite element plane harmonic axisymmetric model, taking into account both the initial make-up torque and the alternating bending load during the test. In these simulations, the most critical stress between the pin or box, in terms of fatigue, mainly depended on the preload. The modelled contact behaviour of the incomplete threads of the box played a significant role in predicting the position of the crack initiation thread root, which was then compared with the test results.

Keywords: axisymmetric finite element analysis; drill collar fatigue tests; fatigue crack propagation; full scale resonant test rig; rotary shouldered threaded connection.

*Corresponding author: Ciro Santus
Ph. +39 (0)50 2218007
Email address: ciro.santus@ing.unipi.it (C. Santus)

1. Introduction

Drill collars are usually placed at the lower part of drill strings and, similarly to drill pipes, can experience large lateral bending loads, induced by string vibration and/or rotation inside a bent path, leading to possible fatigue failures [1, 2, 3, 4, 5, 6, 7]. These loadings are exacerbated by the extreme operating conditions that can be found, for example, in deep-sea drilling for scientific explorations and geological surveys. Inoue et al. [8, 9] described the scientific drilling vessel Chikyu owned by the Japanese research institute JAMSTEC and reported the cumulative fatigue damage analysis performed for the Japan Trench Fast Drilling Project (JFAST) to reach the deep earthquake zone at 1000 m below the seafloor at water depths of around 7000 m. The drill pipe fatigue and the interaction with other kinds of load during the operation, such as the axial dynamic tension induced by the wave motion, were analysed with a probability approach [10]. The possible use of higher strength steels S155 and S160, instead of the more common S150, was therefore investigated by Inoue et al. [11, 12] for this harsh environment.

Resonant test rigs are based on the principle that the lowest natural mode of a mechanical system, for example the first bending mode in a beam-like structure, can be easily excited by a driven vibrating inertial device, and a dedicated control system can keep the stress amplitude steady during the entire fatigue test [13]. A resonant test rig is commonly used for large diameter pipe-like components, such as drill string elements [14, 15, 16], for two main reasons. Firstly, the working frequency can be driven in the range of $20 - 30$ Hz, instead of a value lower than 10 Hz obtained with a quasi-static supporting structure [17, 18], which considerably reduces the testing time especially for long runouts. Secondly, the structure required to support the vibrating system can be relatively light. In fact, the inertial dynamic induces a load on the specimen itself, while it does not affect the supporting elements which, conversely, to bend large diameter pipes would be quite cumbersome [19].

Rotating resonant rigs, featuring a spinning eccentric mass attached to one side of the pipe specimen, are usually employed for long pipe structures, and they correctly simulate the rotating feature of the load [15, 16, 20, 21]. On the other hand, heavy drill collar specimens are more easily tested by following an *in-plane* scheme with two couples of eccentric masses at the ends of large bending arms, as reported by Bertini et al. [14].

We used this in-plane configuration to test drill collar connections whose external diameter was 7" and thread connection size was 5-1/2". The test rig is described, along with the setup procedure, and then a fatigue series test results are reported and analysed.

In this work, in order to identify the key factors which drive the fatigue strength of this threaded connection, we first describe the experimental testing and then propose a finite element analysis. The thread geometry naturally involves stress concentrations that need to be taken into account [22]. The load distribution on the threads

can also be optimized [23] by introducing a double shoulder connection rather than the usual single shoulder [24, 25, 26]. In addition, the make-up torque needs to be carefully measured and monitored [27, 28]. The fatigue mean stress at the root of the first engaged thread of the pin is significantly affected by the preload, and an over make-up torque can be applied to introduce beneficial residual stresses [29]. We investigated the effect of the make-up torque, and then identified the thread root where the fatigue crack initiates by considering the modelled contact status of the incomplete threads of the box.

2. Experimental setup

2.1. Resonant test rig

The resonant test rig used for this activity, Fig. 1, was initially designed and manufactured at the Mechanical Department of the University of Pisa between 1995 and 2000. Its working principle and the mechanical design are detailed in [14] where recent results regarding drill collar connections are also described. These results were used as a comparison for the tests presented in the present paper.

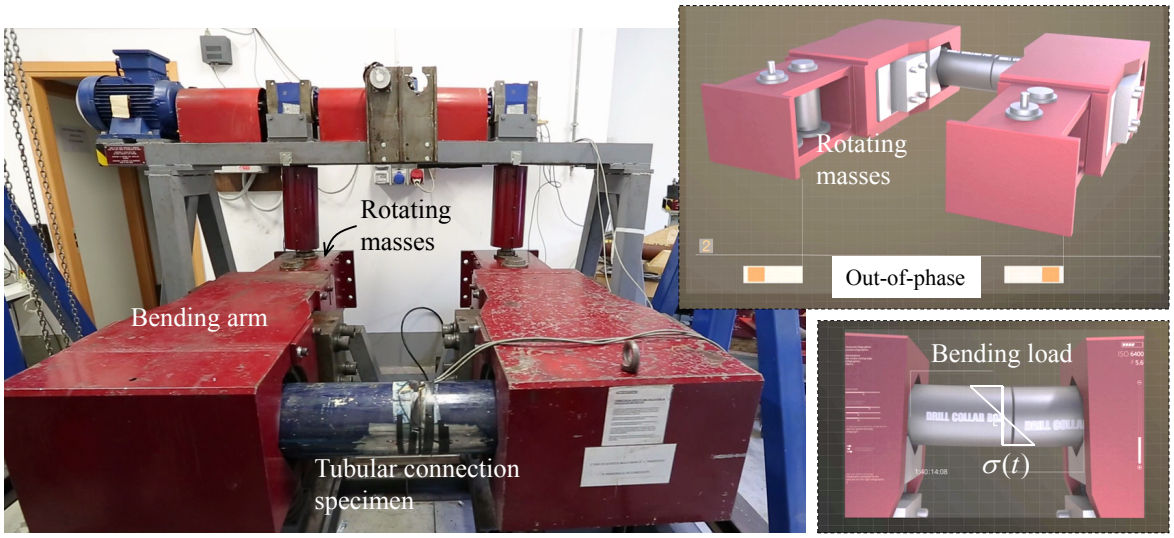

Figure 1: Resonant test rig and drill collar connection specimen, and bending load induced by the out-of-phase eccentric masses.

The resonant principle of the test rig involves two couples of eccentric counter-rotating masses that produce an inertial effect, along the horizontal direction, while the transversal direction forces are neutralized, Fig. 2. The two mass couples can be phase shifted to moderate the applied cyclic bending intensity. Besides this phase tuning, the intensity of the alternating bending can also be controlled by changing the working frequency, as was the case for the tests reported in this paper.

A dynamic parametrization for the bending stress amplitude σ_a can be obtained as a single degree-of-freedom

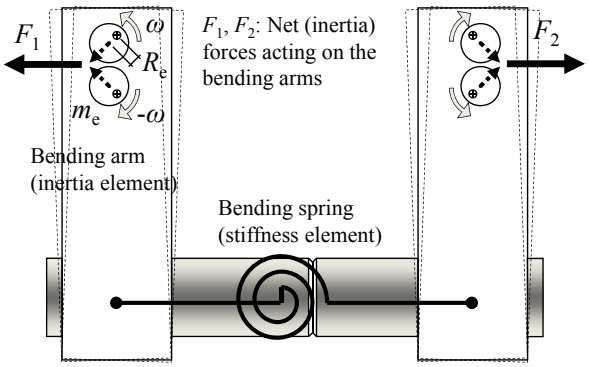

Figure 2: Eccentric rotating mass dynamics, inertia and stiffness components of the test rig.

vibrating model with inertial excitation and viscous damping:

$$\sigma_a \propto \frac{m_e R_e \omega^2}{\sqrt{(1-(\omega/\omega_n)^2)^2 + (2\xi\omega/\omega_n)^2}} \tag{1}$$

where m_e, R_e are the eccentric mass and the eccentricity length respectively, ω is the working angular frequency and ω_n is the natural mode angular frequency, which is the result of the bending stiffness of the pipe specimen and the bending arm moments of inertia. Clearly, having introduced a source of (linear) damping in the model, i.e. a small damping ratio ξ, the stress amplitude is bounded even at the resonance condition ($\omega = \omega_n$), Fig. 3. By keeping the excitation subcritical ($\omega < \omega_n$), the bending load amplitude rapidly increases with the working frequency. This trend was exploited to closed-loop control the stress amplitude during the tests. When the working frequency is driven closer to the resonance, the bending amplitude is higher, and becomes lower when the frequency is not near the natural mode. After a fatigue crack initiation and propagation, the system's natural frequency becomes lower. Therefore, in order to keep a constant alternating loading, the closed-loop control reduces the working frequency, Fig. 3.

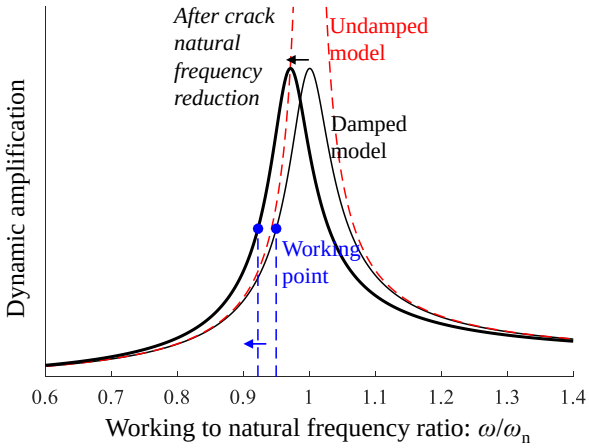

Figure 3: Damped and undamped dynamic models, and working point control after the natural frequency reduction caused by an increasingly larger fatigue crack.

2.2. Strain gauge calibration

The main dimensions of the drill collar rotary shouldered connection and the specification of the material are reported in Fig. 4 (a). Two couples of strain gauges were applied at the external surface of the tested specimen. The two coupled strain gauges were placed on the diametrically opposed bending plane and connected according to the half-bridge configuration. The signal of each couple was the difference between the two opposite strains, thus producing double the signal intensity and also automatically cancelling any temperature deviation. These strain gauges were placed mid way along the thread on the box and relatively far from the connection at the pin, Fig. 4 (b), hereafter referred to as thread and pin strain gauges. Although a specific axial position of the connection within the testing zone was unnecessary, as the bending moment was uniform between the two bending arms, the specimen lengths were set to have the thread strain gauge at half the distance of the test length. Obviously, the thread strain gauge was more sensitive to the presence of a crack in the connection region, and thus was used as a damage sensor. On the other hand, the pipe strain gauge provides an accurate measure of the bending load actually applied to the specimen even after the appearance of a large size crack.

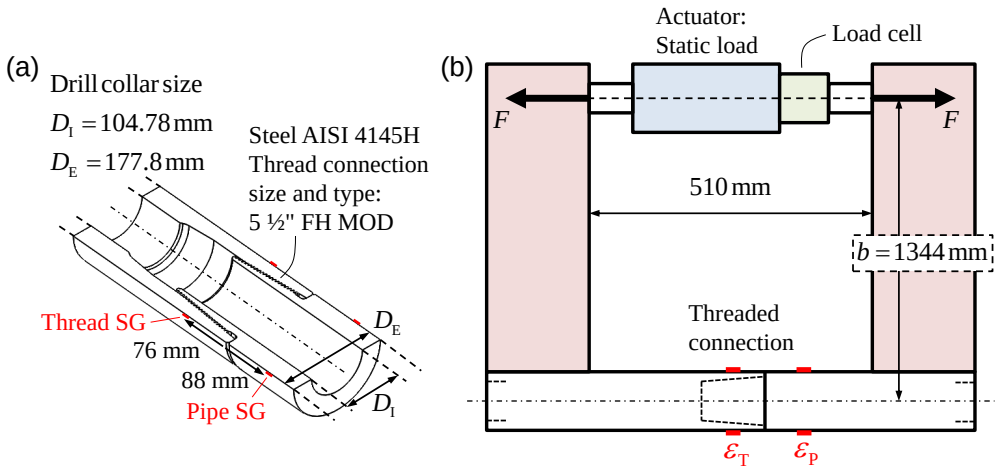

Figure 4: (a) Drill collar rotary shouldered connection dimensions and material. (b) Position of the strain gauges on the connection specimen and setup for the calibration procedure.

Before starting each test, a static strain gauge calibration was performed with the setup shown in Fig. 4 (b). A small hydraulic actuator was used, mounted in series with a pre-calibrated load cell with certified constant K, thus an accurately known bending moment was introduced, and the beam bending stress and strain were easily calculated:

$$F = KF_V, \quad W = \frac{\pi}{32}\frac{D_E^4 - D_I^4}{D_E}, \quad \sigma = \frac{Fb}{W}, \quad \varepsilon = \frac{\sigma}{E} \tag{2}$$

The strain gauges were concurrently measured as voltage signals: E_T, E_P, thread and pipe respectively, to obtain

the strains ε_T and ε_P according to a half-bridge relationship:

$$\varepsilon_T = 2\frac{E_T}{VGk}, \quad \varepsilon_P = 2\frac{E_P}{VGk} \tag{3}$$

where: V is the bridge excitation voltage, G the amplification gain, and k is the gauge factor ($k \approx 2$). These two deformation values showed several percentage points of difference with respect to the strains deduced from the load, Equation 2, and this was ascribed to the uncertainties regarding Young's modulus, the strain gauge factor, the internal thread and the relatively small distance with respect to the bending arm grip. The strain gauge signals recorded were thus directly related to the bending stress deduced from the load, by defining two calibration constants and bypassing Equation 3:

$$C_T = \frac{\sigma}{E_T}, \quad C_P = \frac{\sigma}{E_P} \tag{4}$$

During the dynamic fatigue tests, the two stress values σ_T, σ_P were calculated from the strain gauge signals by means of these two constants, and continuously monitored by an electronic closed-loop control implemented with an Arduino microcontroller.

3. Testing activity

3.1. Fatigue crack detection

At the beginning of the fatigue test, the working frequency was approximately 24 Hz, Fig. 5, and as previously explained, this value was tuned by the controller on the basis of the stress amplitude to be imposed. The frequency remained stable for the entire initiation fatigue life with the thread and pin stresses almost equal. After a sizeable crack affected the connection, the pipe and the thread signals became different and this event was regarded as a reliable initiation detection. In fact, as shown in Fig. 5, the crack appeared on the box's external surface quite near to the position of the thread strain gauge and the position of the crack, reported in Table 1, was very similar in all the tests.

The crack discontinuity reduced the pipe stiffness which in turn lowered the natural frequency ω_n. Hence, in order to keep a specific frequency gap, and keep the controlled stress amplitude stable, the control reduced the working angular speed ω, Fig. 5. Finally, when a quite large crack was obtained, i.e. comparable with half of the pipe section, the working frequency became lower than 10 Hz, and the test was stopped.

In order to provide an effective definition for failure, the in-service usage of the component was considered. The drill collar connection avoids inner pipe leakage, hence a through-wall crack on the box is the limit condition, though the overall structural strength is still relatively high. A similar definition for failure was used by Bertini et al. [14], where the internal pressurization of the tubular specimen allowed a through-wall crack to be detected.

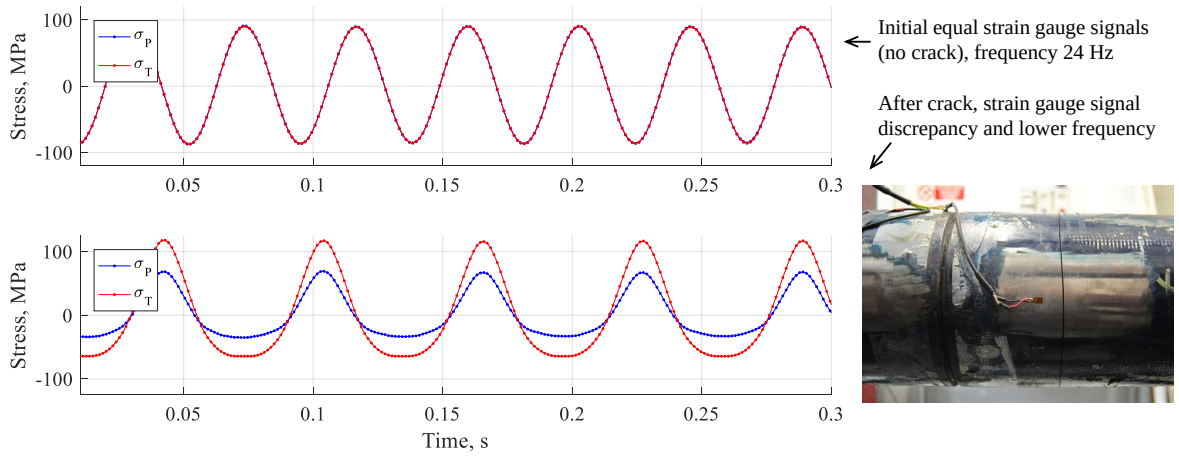

Figure 5: Dynamic strain gauge signal examples, at the beginning of the test (top) and when the connection is affected by a fatigue large crack (bottom).

The last test of the fatigue series was interrupted before the evidence of a large crack. After sectioning the connection, a crack very near to the through-wall condition was found, Fig. 6 (a), and this crack size was assumed to mark the end of the *effective* fatigue life of the tubular component.

Although the path and the shape of the propagated through-wall crack may differ slightly among the various specimens, the corresponding final strain gauge ratio of the last test was taken as a reference for all the other tests, assuming the same crack geometry and the linearity between the strain gauge signals. For example, the end of the effective fatigue life for another specimen (Test 3, Table 1) was obtained as the strain gauge ratio σ_P/σ_T reduced and became equal to the final value of the last test, as shown in Fig. 6 (b). The corresponding number of cycles was recorded as the effective life N_f, while the remaining portion of the test was no longer considered.

3.2. Propagation life correction

During the fatigue experiments, in order to prevent the bending arm lateral displacement from increasing too much, the thread stress was kept constant, whereas the S-N curves were performed with a constant external load. A fracture mechanics correction of the propagation cycles was thus required to obtain the number of cycles corresponding to a through-wall crack as the tests were conducted with constant alternating bending.

The fatigue crack propagation rate was experimentally characterized by following the standard ASTM E647 [30], with C(T) specimens manufactured from a similar hardness drill collar steel. The Rumul Krak-Gage® was used to measure the length of the crack, and the load was applied with a resonant uniaxial testing machine by imposing the load ratio $R = 0.1$. Paris' law model with the threshold correction by Klesnil-Lukáš was fitted to the experimental data, Fig. 7.

The stress intensity factor evolution of a crack in the box component was obtained by means of Finite Element (FE) analyses performed with ANSYS Workbench software. An elliptical crack was initially modelled in a plain

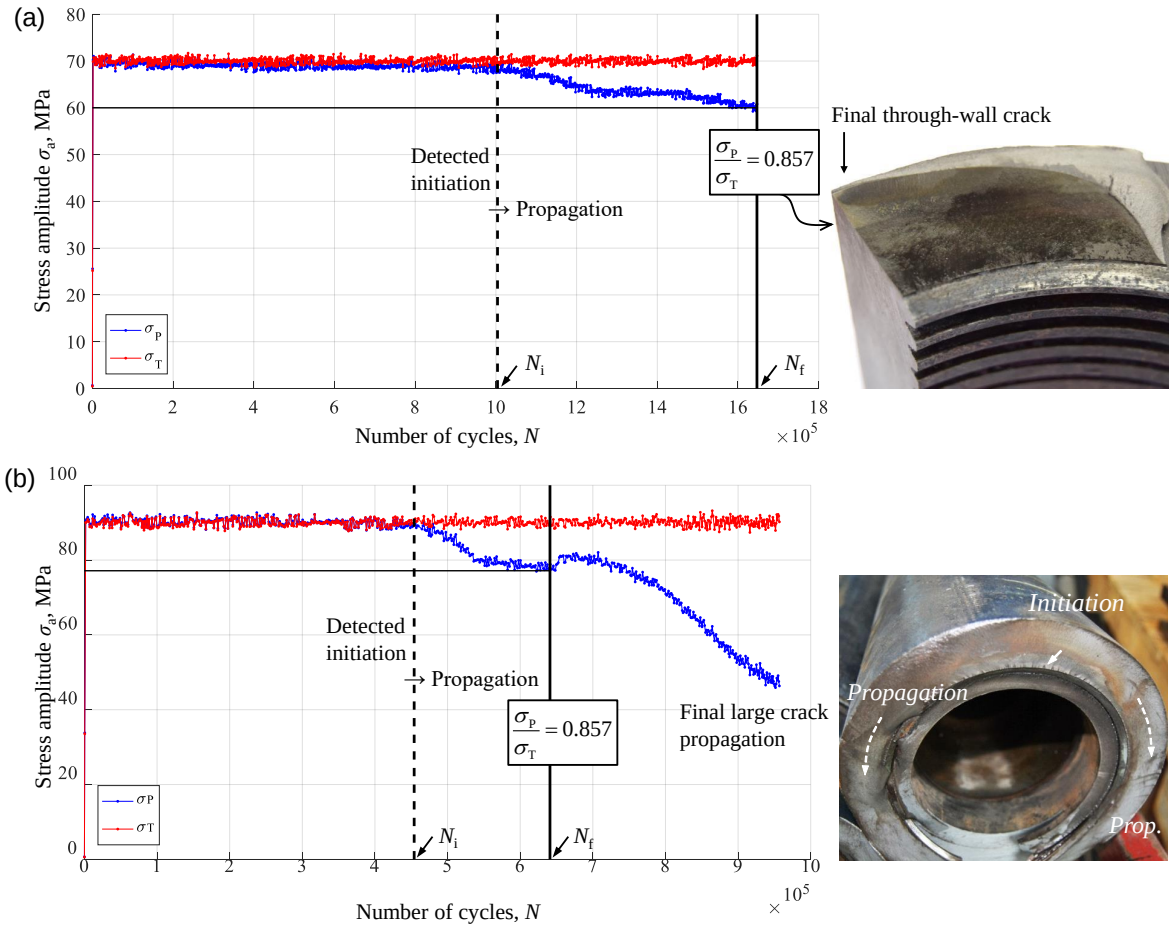

Figure 6: (a) Detected initiation for Test 4 and final strain gauge ratio at the through-wall crack. (b) Detected initiation and number of cycles to effective failure for Test 3 and fracture section after the end of the test.

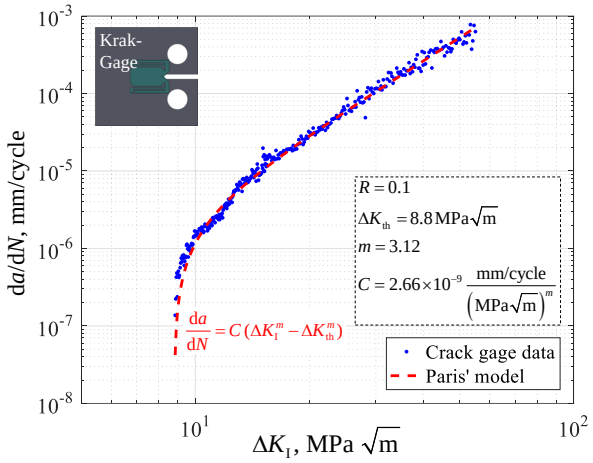

Figure 7: Crack propagation rate data and Paris' law parameters for drill collar steel.

pipe, and the FE procedure was validated by comparing the results with the formulas given in Al Laham and Ainsworth's handbook [31]. A more realistic geometry was then modelled by introducing the crack emanating from a groove at the internal diameter with the same size and shape as the connection thread, and by ranging

several crack sizes to cover the through-wall propagation, Fig. 8. Since no information was available about the shape of the crack during the propagation, a semi-elliptical crack was assumed with the same shape factor as the final crack in Test 4, at least from the detected initiation to the effective failure which was considered as the propagation phase, Fig. 6.

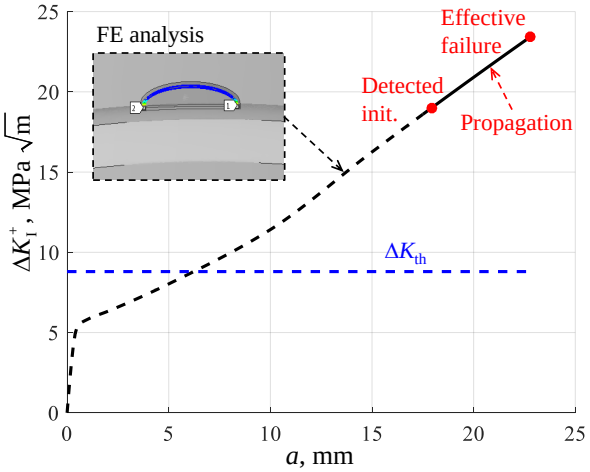

Figure 8: Simulated stress intensity factor evolution for Test 3 and propagation from the detected initiation to the effective failure.

While the load ratio of the fatigue crack growth rate test was $R = 0.1$, the full scale tests were performed at $R = -1$. Therefore, specific crack growth rate data should be obtained at $R = -1$ or at least the Walker equation exploited to apply a correction. However, for a negative load ratio, the Walker equation exponent may be assumed as being zero ($\gamma = 0$) [32], which is equivalent to not considering the compressive portion of the cycle. The crack propagation was therefore calculated with the tensile half cycle of the stress intensity factor ΔK_I^+, which equals the maximum of the K_I cycle, and the experimental data reported in Fig. 7 for a pulsating load.

The average bending stress, measured by the pipe strain gauge, from the detected initiation to the effective failure was evaluated for the propagation analysis, and the initial crack size was back-calculated for each test by setting the actual (experimental) number of cycles for propagation. A crack size of 17 ± 1 mm was obtained, as reported in Table 1. This is quite a large value with respect to the box thickness (22.8 mm in the fracture region) and is consistent with a noticeable deviation of the thread strain gauge measurement.

In order to obtain the corrected number of cycles for propagation, the calculation was repeated on the same crack length range, by assuming a constant bending load up to the through-wall crack size. The corrected numbers of cycles were obviously lower than in the experiments, by approximately $22\% - 25\%$, since the modelled load was higher during the propagation. On the other hand, the initiation was not affected by the control strategy, since the thread and pipe strain gauge signals were initially equal. Therefore, this correction was marginal on the overall number of cycles, since the fatigue life was dominated by initiation.

3.3. S-N test results

The test series results are summarized in Table 1, which reports the initiation position of the box thread root crack L_c with reference to Fig. 10, the detected initiation number of cycles, and the effective and the corrected number of cycles to failure N_f, N'_f. Three tests were performed at 90 MPa, while the fourth connection specimen was tested at 70 MPa and stopped when the crack had reached the through-wall size, as described above.

Table 1: Fatigue test experimental data and crack propagation analysis results.

Test	Amplitude σ_a, MPa	Crack pos. L_c, mm	Det. initiation N_i	Eff. failure N_f	Corrected N'_f	Init. crack a_i, mm
1	90	92	0.784×10^6	1.095×10^6	1.025×10^6	16.0
2[1]	90	91	0.312×10^6	0.491×10^6	0.491×10^6	17.2
3	90	93	0.454×10^6	0.641×10^6	0.600×10^6	17.9
4	70	92	1.004×10^6	1.647×10^6	1.487×10^6	16.8

This S-N data was then compared to the results previously published by Bertini at al. [14] on a similar size drill collar connection NC50, referring to the standard API Spec. 7 [33]. The effective fatigue life, as defined here, up to the event of the through-wall crack, was obtained with an internal pressurization detection procedure. The strength of the connection was very similar to the previous one, as evident in Fig. 9. The fit line was just slightly lower, but this difference can be considered marginal if the usual fatigue scatter is taken into account.

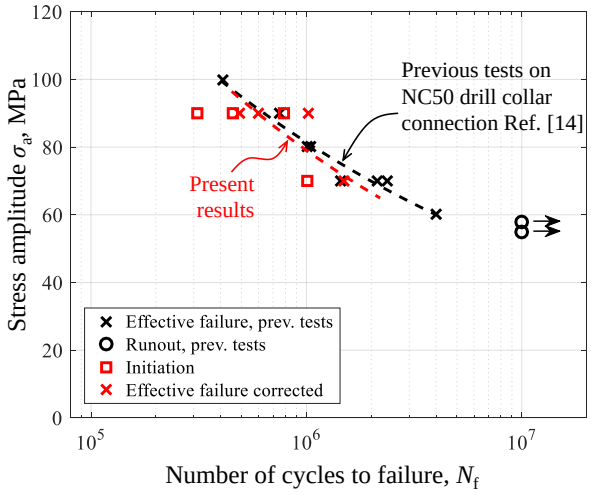

Figure 9: S-N fatigue data of the present tests and comparison with previously published results of a similar size drill collar connection.

3.4. Identification of the critical thread root

The investigation of the fractured connections highlighted that all the specimens experienced the fatigue crack initiation at the region of the final engaged threads of the box, Fig. 10, and the initiation fatigue crack

[1] During Test 2, the pipe stress σ_P was controlled up to the effective failure.

position, reported in Table 1, was $L_c = 92 \pm 1$ mm. The crack initiation and the first propagation was on the box element. The pin also experienced a fatigue crack, in approximately the same axial position and again starting from the thread root, however, only after the box crack had reached the through-wall size. The position where the crack had been detected was not in correspondence to the Last Engaged Thread (LET), as is usually expected for the tool joint threaded connections [34]. In fact, the crack initiated at the position where the box inner diameter was no longer following the conical profile, hence generating some final *incomplete* threads. The load transferred by these incomplete thread flanks was expected to be lower than the regular flanks, and this was considered the reason for the smaller thread root stresses that did not cause critical fatigue loading.

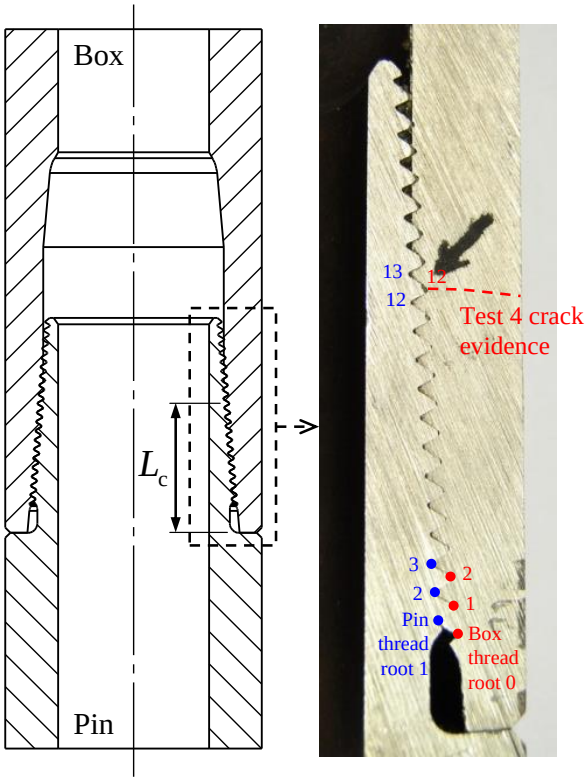

Figure 10: Test 4 connection section, crack evidence, and definition of the thread root initiation position.

4. Fatigue strength analysis of the connection

4.1. Finite element model

The role of these incomplete box threads was investigated with a FE analysis. In order to obtain an accurate resolution, especially at the thread roots, the threaded components are usually approximated with a plane axisymmetric model, rather than a full three-dimensional geometry which is too heavy from the computational point of view. Following this approach, the helical feature was neglected and the threads were approximated as a series of groove rings. Given that the crack had not initiated at the (nominal) LET, but at the last engaged thread

with *complete* shape, Fig. 10, the final incomplete threads were modelled as disengaged, whereas all the other thread flanks were modelled in contact and managed as coupled degree of freedom constraints, Fig. 11.

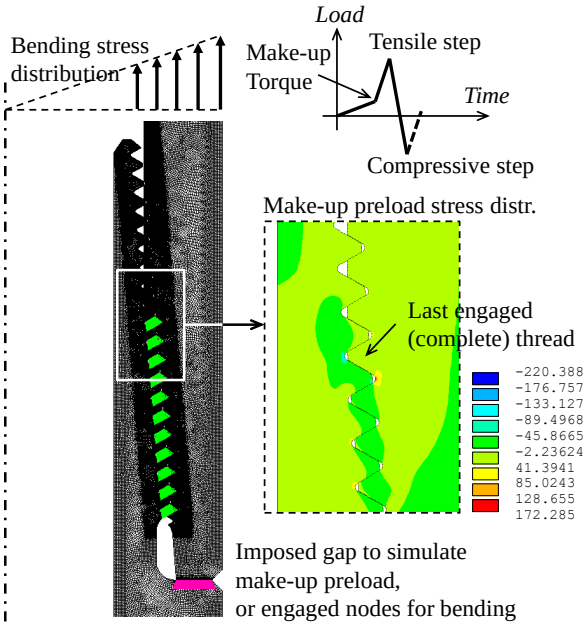

Figure 11: FE plane harmonic axisymmetric model, stop face and thread flank contacts, and simulated loads.

The connection was initially preloaded by the make-up torque, which generates a stress distribution compressive on the box while tensile on the pin. Within the framework of the plane axisymmetric model, the make-up preload was simulated by introducing a controlled gap at the stop face. A unitary gap was preliminarily applied and the contact stress distribution at the threads and at the stop face obtained. The corresponding make-up torque was then calculated by integrating the obtained contact forces multiplied by the average radial positions of the contacts and the coefficient of friction. In order to get the calculated moment equal to the known make-up torque, the stop face gap was then linearly scaled and the preload stress distribution was obtained with this scaled gap value. One reason for uncertainty is the coefficient of friction (CoF), which is approximately 0.3 for dry metal-to-metal, whereas a specific lubricating compound is usually spread on drill collar and tool joint threads, thus reducing the CoF value to approximately 0.15, though with a large scatter [35]. This latter value was used in the present FE analysis, however, if the actual friction is lower, a stronger stress preload is obtained on the basis of the same make-up torque, while on the contrary, with a higher friction the preload is lower.

The tensile and the compressive load steps of the bending cycle, were then simulated with the plane axisymmetric first harmonic. They were then superimposed on the preload stress distribution previously found. A simulation algorithm was implemented to track the contact losses, for both the tensile and compressive steps. In order to keep the analysis linear, the load ramp was fractioned into several contributions, each with a fixed contact

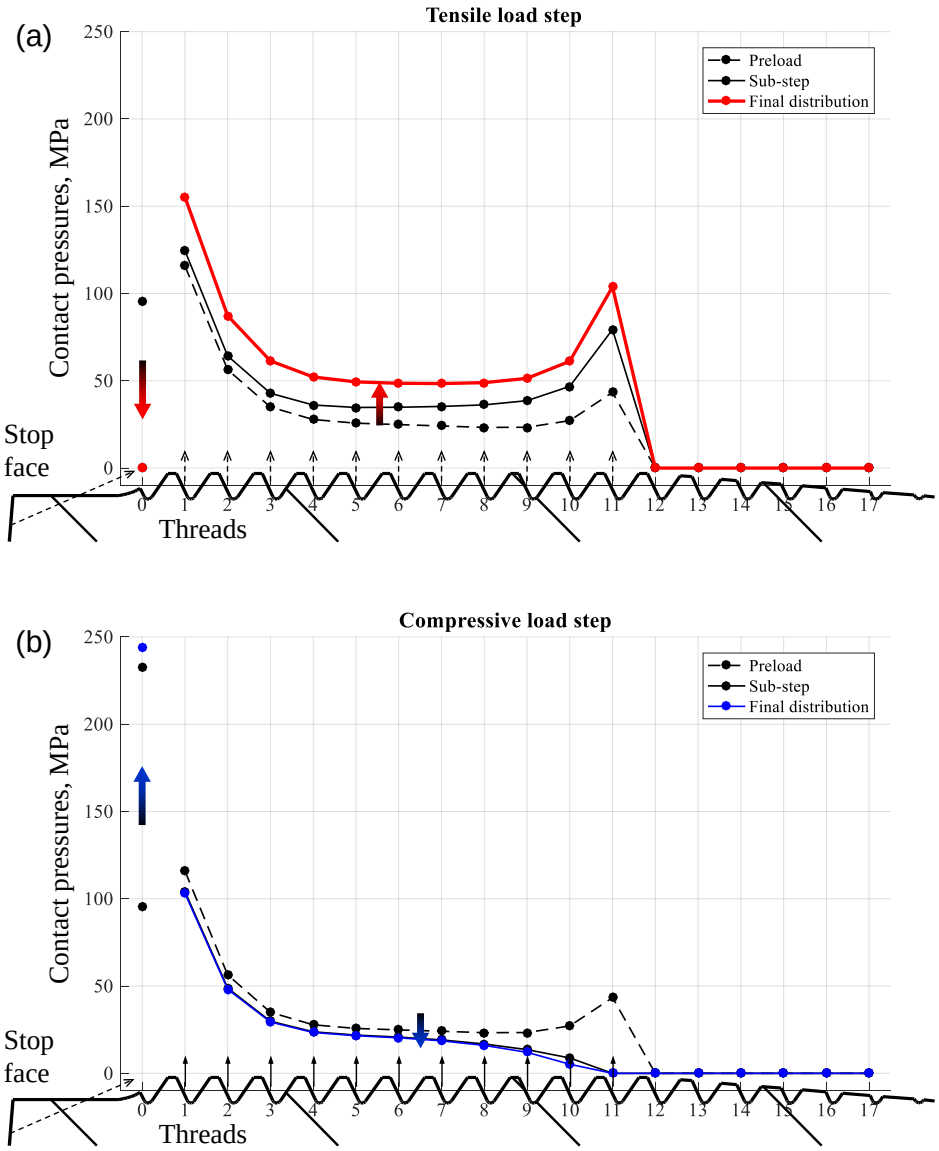

Figure 12: FE contact pressure distributions and evidence of contact losses for bending tensile load step (a) and bending compressive load step (b), after the make-up preload.

pattern. These load fractions were assessed by checking the pressure drop of each single thread. When the tensile half-cycle was analysed, the threads experienced an increase in contact pressure, however, the stop face initially underwent a pressure drop and then a contact loss. The intermediate step reported in Fig. 12 (a) refers to the onset of the contact loss at the stop face, which in turn caused a higher loading rate on the threads. On the other hand, when simulating the compressive bending half-cycle, the stop face experienced an increase in contact pressure, due to the concurrent direction of the load, while the LET underwent contact loss, Fig. 12 (b).

4.2. Thread root fatigue stresses

The same load fractions as the bending tensile and the compressive steps were applied to calculate the local stress histories at the thread roots. The alternating and the mean stresses of pin and box thread roots (enumerated

as in Fig. 10) were obtained and compared to Goodman's line, Fig. 13, which was assessed for the drill collar steel 4145H with tensile strength 150 psi [36].

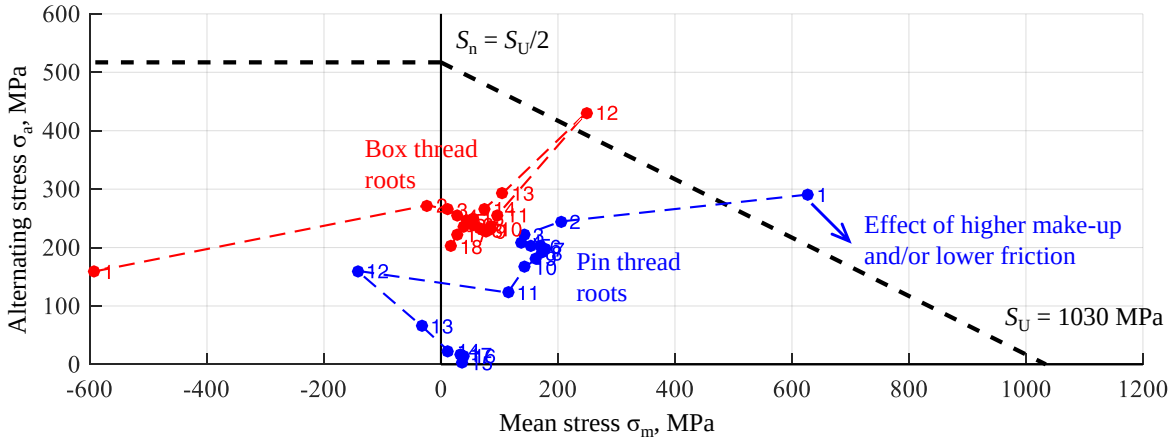

Figure 13: Alternating and mean stresses of the pin and box thread roots compared to Goodman's line of the drill collar steel.

The highest alternating stress was obtained at the root of the box LET with complete profile, where the fatigue fracture was found during the experiments. However, if the incomplete thread contacts were also modelled as engaged, the root of the last thread, though partial, would be the most loaded (for the sake of brevity Goodman's graph is not reported for this case). The assumption of inappropriate load transfer by the incomplete threads was therefore considered acceptable.

The root of the First Engaged Thread (FET) of the pin did not experience the highest alternating stress, but a comparable critical mean and alternating stress combination. A sensitivity analysis, performed with the proposed model, showed a strong influence of the make-up torque on both the mean and alternating stresses at this point, whereas it was less evident on all the other thread roots. In fact, after the stop face contact loss, the maximum stress significantly increases here, since this thread root is the most exposed to the bending load without the shielding from the stop face itself. In spite of a higher mean stress due to the tensile preload, a stronger make-up torque causes a later contact loss during the bending tension ramp, and thus a lower alternating stress at this point. A lower CoF at the threads and at the stop face during the make-up, similarly induces a higher preload, and again less critical stresses at the root of the pin FET. This could explain the failure at the box element, though point 1 of the pin is apparently more critical in Goodman's graph in Fig. 13. An alternative explanation is that there may be ductile relaxation at the pin thread root. In fact the mean stress is quite high with respect to the yield strength, as found by Bertini et al. for a quenched and tempered steel under high load ratio [37].

5. Conclusions

A fatigue test series on 5-1/2" FH MOD drill collar connections was performed with a dedicated test rig which exploits the resonance of a dynamic mechanical system in which the specimen is the stiffness element. The main conclusions of this work are:

- Specific positions of the strain gauges along the connection specimen were able to identify the relevant stages of the crack propagation by considering the evolution of the measurement responses.
- The through-wall crack size on the box element was defined as the effective fatigue failure condition, and a specific strain gauge ratio was then obtained to find the number of cycles at that crack length.
- A fracture mechanics model, based on experimental fatigue data and finite element calculation, was used to predict the propagation up to the through-wall condition, and the minimum size of a crack on the box element, detectable from the strain gauge monitoring, was found.
- The experimental S-N data were compared to the results of a similar size drill collar connection, previously tested on the same resonant rig, and the fatigue lines were almost in total agreement.
- Thread contact losses during the fatigue load cycle were determined with a harmonic plane axisymmetric finite element analysis by superimposing the bending load on the contact distribution initially introduced by the make-up torque.
- In order to correctly predict the crack initiation position, the thread flank contacts modelled had to be limited up to the LET with a complete geometry, and the final incomplete threads disregarded. For this reason, these incomplete threads were unable to correctly transfer the contact load.
- The root of the pin FET was a critical fatigue initiation point, hence in competition with the LET of the box. However, no fatigue fracture was found on the pin element for this connection. The finite element analysis highlighted the strong influence of the make-up torque and the coefficient of friction on the initial stress distribution. The make-up preload affected both the mean and the alternating stresses, especially for the FET of the pin, thus a specific monitoring of the make-up operation is recommended for an accurate fatigue initiation prediction.

References

[1] M.-T. Albdiry, M.-F. Almensory, Failure analysis of drillstring in petroleum industry: A review, Engineering Failure Analysis 65 (2016) 74–85. doi:10.1016/j.engfailanal.2016.03.014.

[2] S.-M. Zamani, S.-A. Hassanzadeh-Tabrizi, H. Sharifi, Failure analysis of drill pipe: A review, Engineering Failure Analysis 59 (2016) 605–623. doi:10.1016/j.engfailanal.2015.10.012.
[3] S. Moradi, K. Ranjbar, Experimental and computational failure analysis of drillstrings, Engineering Failure Analysis 16 (3) (2009) 923–933. doi:10.1016/j.engfailanal.2008.08.019.
[4] M. Ferjani, D. Averbuch, A. Constantinescu, A computational approach for the fatigue design of threaded connections, International Journal of Fatigue 33 (4) (2011) 610–623. doi:10.1016/j.ijfatigue.2010.11.006.
[5] R.-W. Tucker, C. Wang, On the effective control of torsional vibrations in drilling systems, Journal of Sound and Vibration 224 (1) (1999) 101–122.
[6] R.-W. Tucker, C. Wang, An integrated model for drill-string dynamics, Journal of Sound and Vibration 224 (1) (1999) 123–165.
[7] Y.-Z. Zhang, J.-M. Zhang, Z.-J. Shi, Application and development of numerical simulation for underground horizontal directional drilling, Journal of Coal Science and Engineering 18 (1) (2012) 101–107. doi:10.1007/s12404-012-0117-9.
[8] T. Inoue, K. Wada, E. Miyazaki, T. Miyazaki, Scientific Drilling Program of Drilling Vessel Chikyu and Drilling Data Acquisition for Future Technical Development, in: Proceedings of the International Conference on Offshore Mechanics and Arctic Engineering - OMAE, Vol. 5, 2011, pp. 177–183. doi:10.1115/OMAE2011-50090.
[9] T. Inoue, M. Kyo, K. Sakura, Fatigue Strength Evaluation of Drill Pipe for Challenging Deep Drilling Project - Japan Trench Fast Drilling (JFAST), in: Proceedings of the International Offshore and Polar Engineering Conference, 2013, pp. 128–134, ISBN: 978-188065399-9.
[10] T. Inoue, M. Kyo, K. Sakura, T. Fukui, Fatigue Strength Investigation of Drill Pipe for Challenging Scientific Deep Drilling and Utilization of Drilling Data to Estimate Cumulative Fatigue, in: Proceedings of the Annual Offshore Technology Conference, Vol. 1, 2014, pp. 654–665, ISBN: 01603663.
[11] T. Inoue, M. Kyo, T. Miyazaki, K. Sakura, T. Fukui, Superior High-Strength Drill Pipe Adopted in Harsh Environment, in: Society of Petroleum Engineers - SPE International Conference and Exhibition on Oilfield Corrosion, 2012, pp. 124–130, ISBN: 978-162276080-0.
[12] T. Inoue, M. Kyo, K. Sakura, T. Fukui, Drill String Strength Evaluation for Deep Earthquake Zone Drilling, in: Proceedings of the International Conference on Offshore Mechanics and Arctic Engineering - OMAE, Vol. 1, 2012, pp. 691–697. doi:10.1115/OMAE2012-83965.
[13] C.-M. Schabron, J.-A. Puckett, Fatigue testing of traffic signal structures using an eccentric-mass oscillator, Journal of Testing and Evaluation 39 (5) (2011) 1–11. doi:10.1520/JTE103319.
[14] L. Bertini, M. Beghini, C. Santus, A. Baryshnikov, Resonant test rigs for fatigue full scale testing of oil drill string connections, International Journal of Fatigue 30 (6) (2008) 978–988. doi:10.1016/j.ijfatigue.2007.08.013.
[15] F. Xiaoming, Y. Zhichao, W. Liquan, H. Yuxuan, Experiment and finite analysis on resonant bending fatigue of marine risers, Open Mechanical Engineering Journal 9 (1) (2015) 205–212. doi:10.2174/1874155X01509010205.
[16] W. Chuan, H. Zhu, D. Wang, Test System and Model for Fatigue Performance Evaluation of Marine Riser, Journal of Applied Sciences 13 (6) (2013) 854–861. doi:10.3923/jas.2013.854.861.
[17] G.-F. Miscow, P.-E.-V. De Miranda, T.-A. Netto, J.-C.-R. Plácido, Techniques to characterize fatigue behaviour of full size drill pipes and small scale samples, International Journal of Fatigue 26 (6) (2004) 575–584. doi:10.1016/j.ijfatigue.2003.10.014.
[18] Y. Oku, M. Sugino, Y. Ando, T. Makino, R. Komoda, D. Takazaki, M. Kubota, Fretting fatigue on thread root of premium threaded connections, Tribology International 108 (2017) 111–120. doi:10.1016/j.triboint.2016.10.021.
[19] C. Zanuy, P. De La Fuente, M. Pinilla, Bending strength of threaded connections for micropiles, Journal of Constructional Steel Research 78 (2012) 68–78. doi:10.1016/j.jcsr.2012.06.009.
[20] C. Santus, Fretting fatigue of aluminum alloy in contact with steel in oil drill pipe connections, modeling to interpret test results, International Journal of Fatigue 30 (4) (2008) 677–688. doi:10.1016/j.ijfatigue.2007.05.006.
[21] J. Van Wittenberghe, P. De Baets, W. De Waele, W. Ost, M. Verstraete, S. Hertelé, Resonant bending fatigue test setup for pipes with optical displacement measuring system, Journal of Offshore Mechanics and Arctic Engineering 134 (3) (2012) 031702–1 – 6. doi:10.1115/1.4005182.
[22] A.-R. Shahani, S.-M.-H. Sharifi, Contact stress analysis and calculation of stress concentration factors at the tool joint of a drill pipe, Materials and Design 30 (9) (2009) 3615–3621. doi:10.1016/j.matdes.2009.02.022.
[23] X. Zhu, D. Lin, J. Li, Failure analysis and structure optimization of the connecting thread of driving shaft in positive displacement motor, Advances in Mechanical Engineering 8 (6) (2016) 1–11. doi:10.1177/1687814016652313.
[24] Y. Wang, B. Xia, Z. Wang, C. Chai, Model of a new joint thread for a drilling tool and its stress analysis used in a slim borehole, Mechanical Sciences 7 (2) (2016) 189–200. doi:10.5194/ms-7-189-2016.
[25] T. Lin, Q. Zhang, Z. Lian, Y. Liu, Y. Zhang, Y. Chen, Multi-axial fatigue life prediction of drill collar thread in gas drilling, Engineering Failure Analysis 59 (2016) 151–160. doi:10.1016/j.engfailanal.2015.09.012.
[26] Z. Yong, G. Lian-Xin, Y. Peng-Bin, Force analysis and tightening optimization of gas sealing drill pipe joints, Engineering Failure Analysis 58 (2015) 173–183. doi:10.1016/j.engfailanal.2015.08.032.
[27] T. Galle, W. De Waele, J. Van Wittenberghe, P. De Baets, Evaluation of a numerical model for tapered threaded connections subjected to combined loading using enhanced experimental measurement techniques, Journal of Strain Analysis for Engineering Design 50 (8) (2015) 561–570. doi:10.1177/0309324715598916.
[28] T. Galle, J. De Pauw, W. De Waele, J. Van Wittenberghe, P. De Baets, Validating numerically predicted make-up of threaded connections using digital image correlation and infrared monitoring, Journal of Strain Analysis for Engineering Design 49 (7) (2014) 492–500. doi:10.1177/0309324714533328.
[29] I. Korin, J. Perez Ipiña, Controlled residual stresses introduction to improve fatigue resistance of rotary shouldered con-

nections used in oil drilling industry, International Journal of Pressure Vessels and Piping 87 (12) (2010) 696–703. doi:10.1016/j.ijpvp.2010.10.005.
[30] ASTM International, Standard Test Method for Measurement of Fatigue Crack Growth Rates, E647 – 15 (2015). URL http://www.astm.org/Standards/E647
[31] S. Al Laham, R.-A. Ainsworth, Stress Intensity Factor and Limit Load Handbook, British Energy Generation Ltd, 1999.
[32] N. Dowling, Mechanical Behavior of Materials, 4th Edition, Pearson, 2012, iSBN: 9780273764557.
[33] American Petroleum Institute. API Spec. 7, Specification for rotary drill stem elements, 40th ed. (March 2002). URL http://www.api.org/
[34] S. Luo, S. Wu, Effect of stress distribution on the tool joint failure of internal and external upset drill pipes, Materials and Design 52 (2013) 308–314. doi:10.1016/j.matdes.2013.05.073.
[35] C. Santus, L. Bertini, M. Beghini, A. Merlo, A. Baryshnikov, Torsional strength comparison between two assembling techniques for aluminium drill pipe to steel tool joint connection, International Journal of Pressure Vessels and Piping 86 (2-3) (2009) 177–186. doi:10.1016/j.ijpvp.2008.09.007.
[36] Böhler Uddeholm, 4145H Modified API Spec. 7, http://www.buau.com.au/high-tensile.php. URL http://www.buau.com.au/high-tensile.php
[37] L. Bertini, L. L. Bone, C. Santus, F. Chiesi, L. Tognarelli, High Load Ratio Fatigue Strength and Mean Stress Evolution of Quenched and Tempered 42CrMo4 Steel, Journal of Materials Engineering and Performance 26 (8) (2017) 3784–3793. doi:10.1007/s11665-017-2845-x.